npj | precision oncology

Article

Published in partnership with The Hormel Institute, University of Minnesota

https://doi.org/10.1038/s41698-025-01184-1

Adipocyte-driven STAT3-ANGPT2-PTGIS axis promotes cutaneous metastasis in breast cancer and represents a targetable pathway

Chi-Wen Luo[1], Fu Ou-Yang[2], Shu-Jyuan Chang[3], Cheng-Che Wu[1], Yi-Zi Chen[3], Yu-Tzu Yang[3], Mei-Chiang Hsu[3], Sin-Hua Moi[3], Yu-Hsuan Hung[4], Wan-Ling Chu[2], Yen-Liang Li[5], Wen-Chun Hung[5], Chun-Chieh Wu[6], Ming-Feng Hou[1,7], Shu-Yi Lin[8], Wei-Peng Li[9] & Mei-Ren Pan[3,7] ✉

Cutaneous metastatic breast cancer (CMBC) exhibits aggressive behavior driven by tumor adaptation to the skin microenvironment, yet research specifically addressing breast cancer metastasis to the skin remains limited, representing a significant unmet clinical need. In this study, transcriptomic profiling, functional assays, and mouse models revealed that CMBC is associated with poor prognosis and upregulation of angiogenesis, inflammatory signaling, and lipid metabolism, particularly arachidonic and linoleic acid pathways. Adipocyte-derived signals enhanced cutaneous metastasis through STAT3 activation, leading to increased *Angpt2*, *Vegfc*, and *Ptgis* expression. Pharmacologic inhibition of STAT3 suppressed metastasis in vitro and in vivo. Elevated STAT3, ANGPT2, and PTGIS levels correlated with reduced progression-free and disease-free survival. These findings highlight STAT3-mediated signaling and metabolic reprogramming as key drivers of CMBC progression and suggest a promising therapeutic target for this understudied and clinically challenging condition.

Distant metastasis is the leading cause of mortality in patients with breast cancer, with bone, lung, liver, and brain metastases considered to be significant contributors. However, cutaneous metastasis (CM) occurs in nearly 20% of patients with breast cancer, irrespective of the subtype[1,2], and represents a substantial clinical challenge. Notably, approximately 70% of CMs in women originate from breast cancer[3–5]. Moreover, CM in breast cancer is considered a form of local or regional metastasis; therefore, cases with only CM and no distant organ involvement are uncommon. CM primarily progresses through angiogenesis and lymphangiogenesis, processes involving new blood and lymphatic vessel formation, facilitating cancer cell dissemination to the regional lymph nodes and beyond[6–9]. Consequently, anti-angiogenic drugs have emerged as the first-line treatment for metastatic breast cancer involving the skin. However, drug resistance remains a significant limitation, often leading to treatment failure.

Recent studies have underscored the critical role of chemoattractant signaling in orchestrating breast cancer metastasis. These signaling pathways, mediated by interactions between chemokines and their corresponding receptors, guide cancer cells toward specific microenvironments such as the lung, lymph nodes, and skin. Among them, the CXCR4-CXCL12 axis has been extensively characterized: CXCL12, secreted primarily by stromal fibroblasts and pulmonary vascular endothelial cells, acts as a potent chemoattractant for CXCR4-expressing breast cancer cells, enhancing their migration and invasion[10]. Similarly, the CCR7-CCL21 axis drives cancer cells toward lymphatic vessels, facilitating dissemination[11] and further promoting the adhesion, survival, and migration of breast cancer cells in the tumor microenvironment[12]. These chemoattractive pathways direct cancer cells to the target organ by promoting extracellular matrix remodeling, angiogenesis, and lymphangiogenesis, creating a permissive niche for tumor growth and

[1]Division of Breast Oncology and Surgery, Department of Surgery, Kaohsiung Medical University Hospital, Kaohsiung, Taiwan. [2]Wesing Breast Hospital, Kaohsiung, Taiwan. [3]Graduate Institute of Clinical Medicine, Kaohsiung Medical University, Kaohsiung, Taiwan. [4]Center for Cancer Research, Kaohsiung Medical University, Kaohsiung, Taiwan. [5]National Institute of Cancer Research, National Health Research Institutes, Tainan, Taiwan. [6]Department of Pathology, Kaohsiung Medical University Hospital, Kaohsiung Medical University, Kaohsiung, Taiwan. [7]Drug Development and Value Creation Research Center, Kaohsiung Medical University, Kaohsiung, Taiwan. [8]Institute of Biomedical Engineering and Nanomedicine, National Health Research Institutes, Miaoli, Taiwan. [9]Department of Medicinal and Applied Chemistry, Kaohsiung Medical University, Kaohsiung, Taiwan. ✉e-mail: mrpan@cc.kmu.edu.tw

progression[13]. Moreover, obesity amplifies these pathways since adipokines such as leptin (LEP) and interleukin (IL)-6 synergize with chemokine signaling, particularly the CXCR4-CXCL12 axis, to enhance cancer cell migration to specific tissues[14,15]. Despite these advances, the therapeutic targeting of chemoattractive signaling remains an underexplored and promising strategy, especially in patients with CM, for whom effective interventions are limited. Further investigation into these pathways may uncover novel approaches to impede metastatic progression and improve clinical outcomes.

Advances in genetic profiling, such as mutational analyses of CMs, have revealed essential molecular alterations not observed in primary tumors. Yan Xu et al. compared the mutational landscapes of primary tumors and their corresponding lymph nodes or CM tissues using next-generation sequencing of 425 cancer-relevant genes. They found that *TP53* and *PIK3CA* mutations and *TERT* amplification were prevalent in CM tissues and correlated with poor prognoses[16]. Similarly, Schrijver et al. analyzed eight paired cases of skin metastases and identified 33 mutations, including *ATR*, *BRCA1*, *SMAD4*, *CDH1*, *ARID1A*, *ERBB2*, *IDH1*, *PIK3R1*, *RB1*, and others, in skin metastases that were not detected in the corresponding primary breast tumors[17,18]. Moreover, a recent study reported that specific genes, including *JAK2* and *NF1*, appear to be preferentially mutated in metastatic breast cancer. Furthermore, the study identified significantly mutated genes (SMGs), such as *TP53* and *AKT1*, which exhibit a markedly higher mutation frequency in metastatic tumors compared to primary tumors[19]. In another study, *TP53* mutations were detected in 50% of CMs and 31% of lymph node metastases, emphasizing their distinct molecular profiles[18]. These findings highlight the potential of genetic alterations as biomarkers and therapeutic targets in CM.

Therefore, this study aimed to integrate insights from transcriptomic alterations into therapeutic strategies, offering novel approaches for the prevention and management of skin metastases in patients with breast cancer.

Results

CM represents a clinically significant indicator of poor prognosis in breast cancer

To understand the impact of CM from breast cancer on patient survival, we conducted a survival analysis from a retrospective cohort of 126 patients. The cohort included 74 patients followed without recurrence for five years, 36 patients with distant metastases excluding the skin (including lung, liver, and bone), and 16 patients with distant metastases involving the skin. Baseline clinicopathological characteristics at initial diagnosis revealed significant differences among the four patient groups (no metastasis, non-cutaneous metastasis, multiple-organ metastasis, and cutaneous metastasis only), suggesting critical prognostic implications (Fig. 1A). Pathological staging differed significantly across groups ($P < 0.0001$), with patients who eventually developed cutaneous metastasis only showing more advanced disease at baseline: 33.33% were stage IV, and none were stage I. This indicates that patients destined to develop cutaneous metastasis only presented with more aggressive tumor burden from the outset. Similarly, the proliferation index (Ki67) was significantly elevated in the cutaneous metastasis only group ($P = 0.0138$), where 100% of patients had Ki67 values > 20%, suggesting an inherently high proliferative potential. In contrast, patients in the no metastasis group had a much lower rate of high Ki67 expression (55.41%), reflecting a more indolent biological phenotype at diagnosis. Lymphovascular invasion (LVI) was also more prevalent at baseline in patients who later developed cutaneous metastasis only (100%) compared to those with no metastasis (36.99%) and those with non-cutaneous metastasis ($P = 0.0025$). The presence of LVI at diagnosis has

A

Characteristics	No metastasis (%)	Non-cutaneous metastasis n(%)	Multiple-organ metastasis n(%)	Cutaneous metastasis only n(%)	P-value
Case no.	74	36	10	6	
Diagnosed age, year	54 ± 12	50 ± 12	50 ± 13	50 ± 10	0.4132
Clinical stage					**0.0003**
1	27(36.49)	6(16.67)	3(30.00)	0(0.00)	
2	41(55.41)	22(61.11)	3(30.00)	4(66.67)	
3	6(8.11)	7(19.44)	1(10.00)	0(0.00)	
4	0(0.00)	1(2.78)	3(30.00)	2(33.33)	
Pathological stage					**<0.0001**
1	14(18.92)	3(8.33)	2(20.00)	0(0.00)	
2	54(72.97)	23(63.89)	3(30.00)	1(16.67)	
3	6(8.11)	8(22.22)	2(20.00)	3(50.00)	
4	0(0.00)	2(5.56)	3(30.00)	2(33.33)	
Subtype					0.2993
Her2 enriched	15(20.27)	3(8.33)	2(20.00)	1(16.67)	
Luminal A	28(37.84)	23(63.89)	6(60.00)	4(66.67)	
Luminal B	21(28.38)	5(13.89)	1(10.00)	1(16.67)	
TNBC	10(13.51)	5(13.89)	1(10.00)	0(0.00)	
Ki67					**0.0138**
≦20	33(44.59)	7(19.44)	3(30.00)	0(0.00)	
>20	41(55.41)	29(80.56)	7(70.00)	6(100.00)	
Grade					0.8521
1	4(5.41)	1(2.78)	0(0.00)	0(0.00)	
2	39(52.70)	16(44.44)	4(40.00)	2(33.33)	
3	30(40.54)	19(52.78)	6(60.00)	4(66.67)	
Unknown	1(1.35)	0(0.00)	0(0.00)	0(0.00)	
DLI					0.2251
Negative	70(95.89)	34(94.44)	8(88.89)	3(75.00)	
Positive	3(4.11)	2(5.56)	1(11.11)	1(25.00)	
LVI					**0.0025**
Negative	46(63.01)	14(38.89)	7(77.78)	0(0.00)	
Positive	27(36.99)	22(61.11)	2(22.22)	5(100.00)	
PNI					0.2032
Negative	66(90.41)	28(77.78)	8(88.89)	3(75.00)	
Positive	7(9.59)	8(22.22)	1(11.11)	1(25.00)	
Survival status					<0.0001
survived	68(91.89)	17(47.22)	1(10.00)	3(50.00)	
died	6(8.11)	19(52.78)	9(90.00)	3(50.00)	

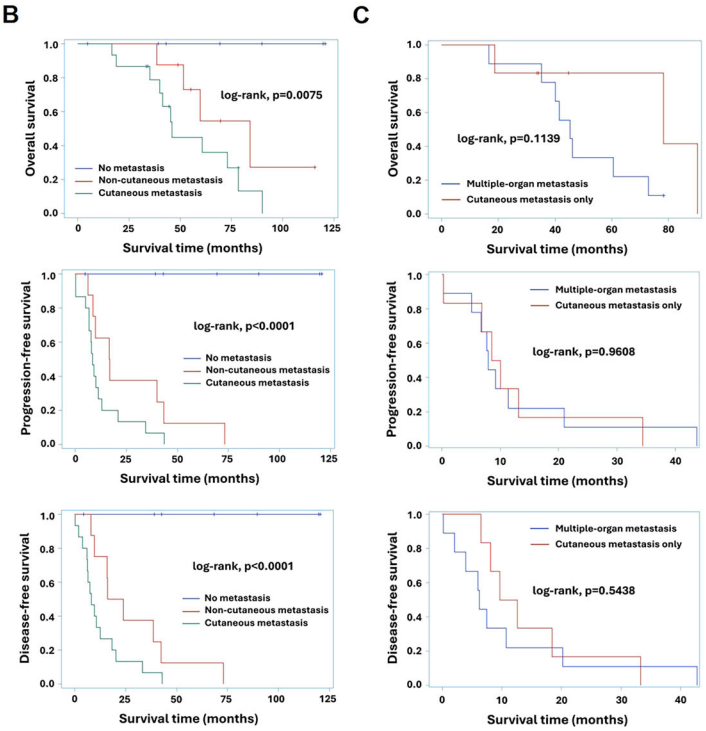

Fig. 1 | CM is associated with reduced survival in breast cancer patients. **A** Baseline characteristics of the KMUH cohort ($N = 126$). **B** Kaplan-Meier survival analysis comparing three patient groups: no metastasis (blue), non-cutaneous metastasis (red), and cutaneous metastasis (green). Overall survival (OS) was significantly lower in patients with cutaneous metastasis compared to those with non-cutaneous metastasis or no metastasis (log-rank test, $P = 0.0075$). Progression-free survival (PFS) and disease-free survival (DFS) were also significantly reduced in the cutaneous metastasis group (log-rank test, $P < 0.0001$). **C** Kaplan-Meier curves comparing OS, PFS, and DFS in breast cancer patients with cutaneous metastasis only (red) versus those with metastases involving multiple-organ metastasis (blue). OS showed a trend toward longer survival in the cutaneous metastasis only group, although the difference did not reach statistical significance (log-rank test, $P = 0.1139$). PFS and DFS were comparable between the two groups, with no significant difference observed (log-rank test, $P = 0.9608$ and $P = 0.5438$).

well-established links to increased metastatic risk, further highlighting the aggressive nature of tumors in the cutaneous metastasis only. Finally, survival outcomes differed markedly among the groups ($P < 0.0001$), with the CM group experiencing the worst prognosis despite their metastases being limited to the skin. This suggests that the initial tumor biology, not merely the site of recurrence, plays a critical role in determining outcomes.

Kaplan-Meier survival analysis was performed to compare outcomes among three patient groups: those without metastasis (no metastasis), those with distant metastases excluding the skin (non-cutaneous metastasis), and those with CM (cutaneous metastasis). Overall survival (OS) was significantly lower in the CM group compared to the non-cutaneous metastasis group ($P < 0.0001$), indicating that skin involvement is associated with poorer survival (Fig. 1B). Similarly, progression-free survival (PFS) and disease-free survival (DFS) were markedly worse in the cutaneous metastasis group, with log-rank $P < 0.0001$(Fig. 1B). These results suggest that CM in breast cancer is linked to more aggressive disease behavior and inferior clinical outcomes compared to non- CM. To further investigate the prognostic implications of CM, we compared patients with cutaneous metastasis only to those with multiple organ metastases. In terms of OS, patients with cutaneous metastasis only showed a trend toward better survival than those with multiple-organ metastasis; however, the difference was not statistically significant ($P = 0.1139$). Similarly, PFS and DFS did not differ significantly between the two groups ($P = 0.9608$ and $P = 0.5438$) (Fig. 1C).

Together, these findings suggest that patients who develop cutaneous metastasis only already exhibit aggressive disease features at diagnosis, including advanced pathological stage, high proliferative index, and vascular invasion, all of which are associated with poorer survival. These baseline parameters support the prognostic value of early tumor profiling in predicting recurrence patterns and long-term outcomes.

Patients with CM exhibited significant angiogenesis in both the primary breast tumor and the metastatic skin tissue

To investigate the underlying phenotype by which CM reflects tumor aggressiveness, we subsequently conducted multi-omics analyses using tissue samples from a patient with triple-negative breast cancer (TNBC) who presented with a solitary cutaneous metastasis only. The initial presentation before treatment showed the patient's clinical baseline without evident skin involvement (Fig. 2A). Following serial chemotherapy and radiation therapy, multiple cutaneous metastatic nodules developed on the left anterior chest wall (Fig. 2B). The patient eventually progressed to extensive cutaneous metastases, presenting as numerous indurated papules and plaques and ulcerated nodules dispersed across both the left and right lateral chest wall regions (Fig. 2C). Figure 2D illustrates the patient's clinical timeline, detailing the sequence of surgical resections. These included the initial tumor in the left breast (Tissue #1), the first cutaneous metastatic lesion (Tissue #2), the recurrent tumor in the right breast (Tissue #3), and the advanced, irreversible CM (Tissue #4-Tissue #6) (Fig. 2D).

CMBC tissues commonly exhibit prominent angiogenesis, which facilitates tumor growth and dissemination. We performed immunohistochemical staining on tissue samples obtained from different treatment stages to investigate the underlying mechanisms further (Fig. 2E). The staining revealed strong lymphangiogenesis marker D2-40 and the angiogenesis marker CD105 expression across all tissue samples. These findings indicate that lymphangiogenesis and angiogenesis are prominent features in the primary tumor and subsequent metastatic sites, suggesting that tumor progression at various stages relies on forming new lymphatic and blood vessels to sustain growth and enable dissemination. The presence of these vascular features in both primary and metastatic sites suggests that targeting tumor vasculature may represent a viable therapeutic strategy for patients with skin-dominant metastatic disease.

Breast cancer cells with CM exhibit enhanced adipogenic and metabolic signaling

To elucidate the molecular characteristics associated with skin invasion in breast cancer, we analyzed RNA-seq data derived from both primary and metastatic tumor tissues. Following data normalization, differential gene expression analysis was performed using DESeq2 to compare the primary and metastatic groups. A total of 1,110 differentially expressed genes (DEGs) were identified (adjusted $P < 0.001$), among which 735 genes were significantly upregulated (adjusted $P < 0.001$, $\log_2$ fold change > 2), and 375 genes were significantly downregulated (adjusted $P < 0.05$, $\log_2$ fold change < -2) (Fig. S1A). Hierarchical clustering and heatmap visualization confirmed that the selected DEGs effectively distinguished between the primary and metastatic tumor profiles (Fig. S1B). As illustrated in Fig. 3A, KEGG pathway enrichment analysis revealed that DEGs were involved in key signaling pathways, including cytokine-cytokine receptor interaction (24 genes), cell adhesion molecules (CAMs, 21 genes), Hippo signaling (17 genes), and pathways regulating stem cell pluripotency (14 genes) (Fig. 3A). Several lipid metabolism pathways were also enriched, such as arachidonic acid (AA), linoleic acid (LA), and alpha-linolenic acid (α-LA) metabolism, indicating their potential roles in membrane remodeling, signal transduction, and inflammation during tumor progression.

Gene Set Enrichment Analysis (GSEA) revealed that metastatic tissues exhibited significant upregulation of several biological pathways compared to primary tumors, including adipogenesis, fatty acid metabolism, angiogenesis, epithelial-mesenchymal transition (EMT), inflammatory response, and interferon-gamma response (Fig. 3B). Complementary Reactome pathway analysis, visualized using SRplot, further highlighted that lipid metabolism and immune-related pathways were among the most dysregulated in cutaneous metastatic tissues relative to primary tumors (Fig. 3C). These results suggest that cutaneous metastatic tissues possess a more aggressive and malignant phenotype, characterized by heightened inflammatory signaling, increased angiogenic activity, enhanced cytokine-cytokine receptor interactions, and altered fatty acid metabolism.

To further investigate the crosstalk between cancer cells, adipocytes, and angiogenesis in the development of CMBC, we isolated cancer cells from patient tissues (Fig. 3D) and co-cultured them with autologous adipocytes derived from adipose-derived stem cells obtained from the same patient (Fig. 3E). To evaluate the pro-angiogenic effects of this tumor-adipocyte interaction, we analyzed the conditioned medium from the co-culture using the RT² Profiler™ Human Angiogenesis PCR Array (Cat. No. 330231 PAHS-024ZA; SA Biosciences, Valencia, CA, USA), which profiles the expression of 84 angiogenesis-related genes. The analysis identified the top five upregulated genes as *LEP*, *Sphingosine-1-phosphate receptor 1* (*S1PR1*), *thymidine phosphorylase* (*TYMP*), *CCL11*, and *CCL2* (Fig. 3F). Among these, *LEP* expression steadily increased along disease progression (Fig. 3G), which was further validated by immunohistochemical staining across serial tumor samples (Fig. 3H) and functionally, conditioned medium from the co-culture significantly enhanced tube formation in endothelial cells, demonstrating potent angiogenic activity (Fig. S2). These findings underscore the role of adipocyte-derived factors in promoting angiogenesis and potentially facilitating metastatic progression in CMBC.

Transcriptomic profiling reveals tumor evolution and increasing heterogeneity across disease progression

To further investigate the molecular evolution of CMBC, we constructed a phylogenetic tree based on transcriptomic data from six tumor samples obtained at distinct time points. As shown in Fig. S3A, gene expression levels increased notably in later-stage tissues (Tissues #4-6), as reflected by elevated log-counts per million (log-CPM) values and a broader distribution, indicating heightened transcriptional activity associated with advanced disease. As shown in Fig. S3B (left panel), Tissue #1 (Breast T1, primary tumor from the left breast) and Tissue #2 (Skin T2, left chest wall skin metastasis) clustered closely, suggesting that these early-stage samples shared similar molecular signatures and gene expression profiles, based on the analysis of 31,533 genes. However, a clear divergence in gene expression patterns emerged as the disease progressed. Later-stage samples, including Tissue #3 (Breast T3, primary tumor from the right breast) and Skin Tissues #4-#6 (T4-T6, skin metastases from the right chest wall), branched distinctly from the early-stage cluster. This phylogenetic branching implies that

A

B

C

D

Label	Tissue	Date	Condition
Tissue#1	Breast	2015/9/16	pre-treatment of left breast
Tissue#2	Skin	2020/5/20	left skin
Tissue#3	Breast	2020/8/3	right breast
Tissue#4	Skin	2020/12/8	skin
Tissue#5	Skin	2021/2/5	skin
Tissue#6	Skin	2021/7/15	skin

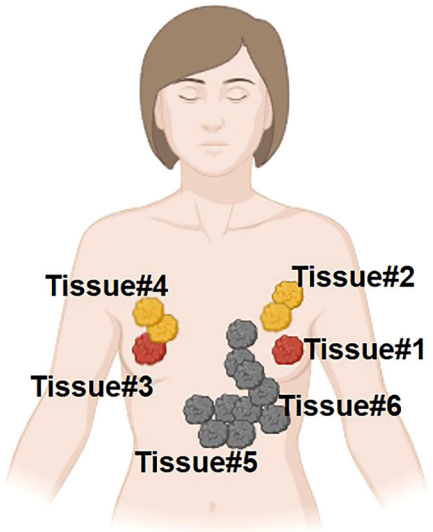

E

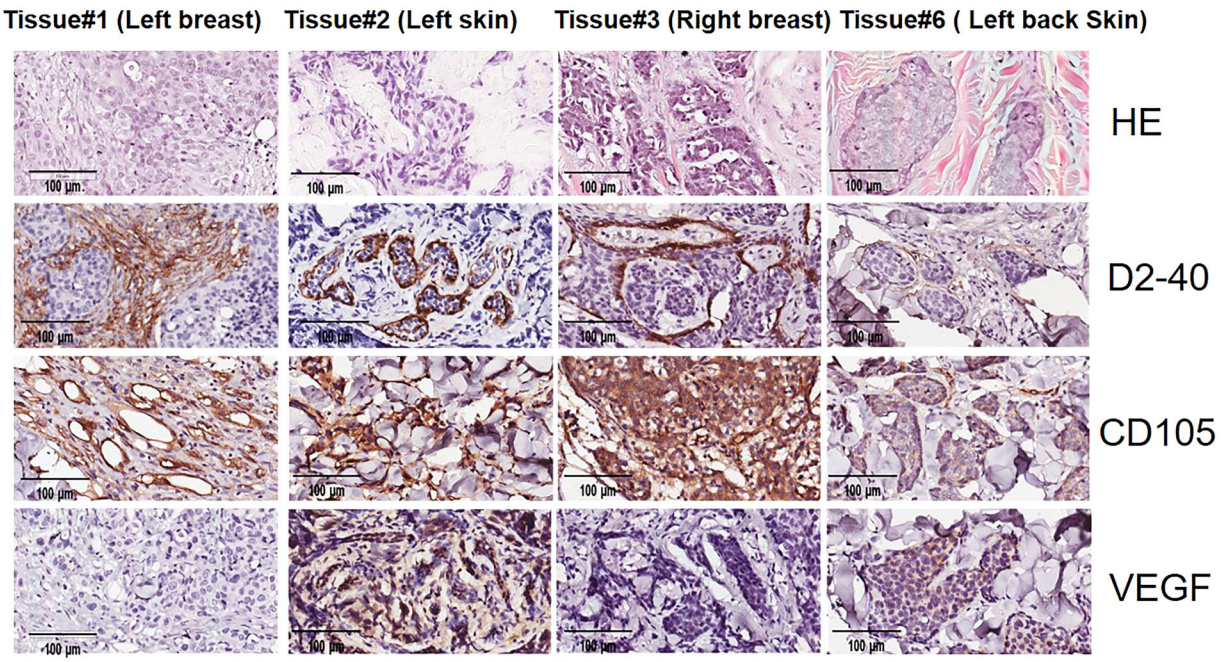

Fig. 2 | CM is associated with increased angiogenic activity in primary tumors and metastatic skin lesions. A A clinical aspect of breast cancer patients before treatment. **B** This shows multi-nodule cutaneous metastases on the left anterior chest after the patient received serial chemotherapy and underwent radiation. **C** The patient exhibited cutaneous metastases characterized by numerous indurated papules and plaques, accompanied by ulcerated nodules distributed across the left and right chest wall extremities. **D** List of six tumor tissues at different time points. **E** HE staining and immunohistochemistry analysis of the breast tumors and the skin nodules. The immunohistochemistry analysis indicated that the breast and skin nodules cells were positive for D2-40, CD105, and VEGF.

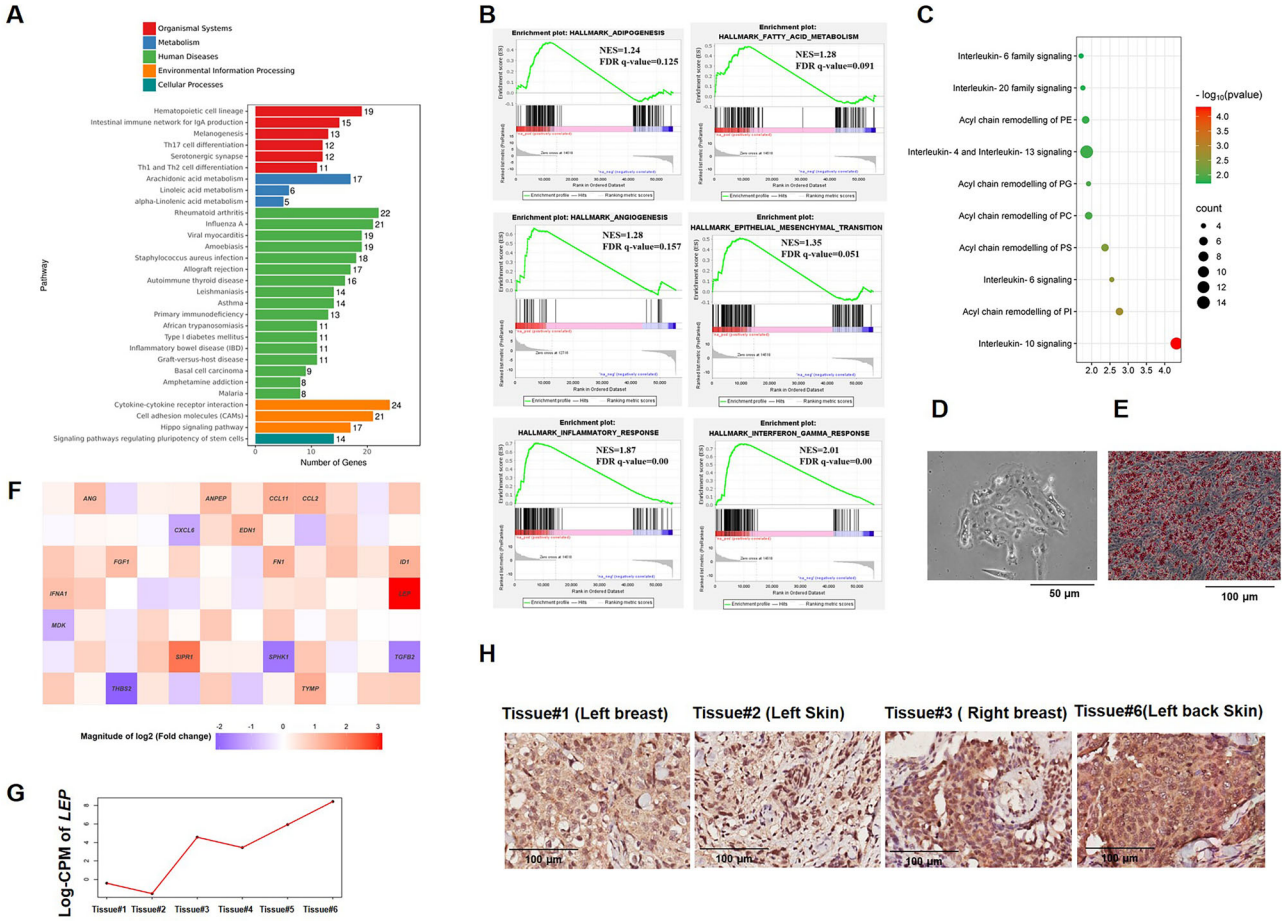

Fig. 3 | KEGG and Gene Set Enrichment Analyses (GSEA) were performed on primary and cutaneous breast cancer tissues. A KEGG analysis of all differentially expressed genes. **B** GSEA compares primary and cutaneous breast cancer tissues in our cohort, with enrichment plots highlighting activated gene sets related to adipogenesis, fatty acid metabolism, angiogenesis, epithelial-mesenchymal transition, inflammatory response, and Interferon Gamma Response. **C** Reactome analysis visualized using SRplot, identified lipid metabolism and immunity as key dysregulated pathways. **D** Microscopic morphology of cancer cells. **E** ASC differentiation into adipose cells. Representative pictures of white adipocytes with oil red O staining. **F** To assess the pro-angiogenic effects of tumor-adipocyte crosstalk, conditioned medium from the co-culture of patient-derived breast cancer cells and autologous adipocytes was analyzed using the RT^2 Profiler™ Human Angiogenesis PCR Array, which profiles 84 angiogenesis-related genes. Fold change of the gene expression levels of 84 angiogenesis-associated genes in tumor cells in a mono-culture (control group) or a co-culture with adipocytes (experimental group) by qPCR array. **G** *Leptin (LEP)* gene expression in tumor tissues across stages, from early (tissue #1) to late (tissue #6). **H** IHC staining of Leptin in the tumor and cutaneous tumor tissues of the patient.

cancer cells undergo substantial transcriptional reprogramming during metastasis, resulting in divergent subtypes with distinct molecular characteristics, underscoring the tumor's adaptability and heterogeneity.

Notably, genes involved in the adipocytokine signaling pathway (35 genes) and fatty acid metabolism (98 genes) were particularly effective in distinguishing tumor samples across different stages (Fig. S3B, center, and right panels). The progressive divergence between early-stage samples (Breast T1 and Skin T2) and late-stage metastatic tissues (Skin T4-T6) highlights the temporal evolution and increasing complexity of tumor cell phenotypes as they adapt to new microenvironments. We further examined the expression of fatty acid metabolism-related genes across tissues collected at six distinct time points (Fig. S3C). A total of 98 genes were analyzed, encompassing those involved in key metabolic processes such as fatty acid β-oxidation and synthesis, arachidonic acid metabolism (including prostaglandin and leukotriene synthesis), cytochrome P450-mediated drug metabolism, the phospholipase A2 (PLA2) signaling cascade (associated with lipid signaling and membrane remodeling), and gamma-glutamyl transpeptidase (GGT) activity (linked to glutathione metabolism and oxidative stress regulation). Among these, 30 genes demonstrated significant differential expression throughout disease progression (Table S1). Specifically, genes such as *PTGS2*, *ACSBG1*, *PTGIS*, *LTC4S*, and *CYP2C8* were markedly upregulated in late-stage tissues, while *PTGES3*, *GPX1*, and *ECHS1* were significantly downregulated compared to the primary tumor tissue. These findings collectively suggest that, as CMBC progresses, tumor cells exhibit enhanced activity in lipid metabolism, prostaglandin biosynthesis, detoxification pathways, and oxidative stress responses. Such alterations may lead to more aggressive and adaptive phenotypes during metastatic spread.

Cutaneous 4T1 cells exhibit elevated expression of angiogenesis-related and adipokine-associated genes

Several studies have suggested that adipocyte-derived (Ad) factors significantly enhance the metastatic potential of 4T1 cells[20,21]. To investigate how adipocyte-derived factors contribute to the skin-specific progression of breast cancer, we exposed 4T1 cells to adipocyte-conditioned medium (Ad-CM). To examine the role of fatty acid metabolism in shaping the tumor microenvironment and its contribution to the recurrence of breast cancer with CM, we utilized a murine model. Clinically, skin metastases frequently emerge following surgical resection of the primary tumor. To mimic this scenario, we examined the effects of adipocyte-conditioned medium (Ad-CM) on tumor progression. As shown in Fig. 4A, treatment with Ad-CM markedly promoted tumor metastasis to additional subcutaneous regions, particularly the cervical, neck, and dorsal areas. Histological analysis using hematoxylin and eosin (H&E) staining confirmed the presence of skin-

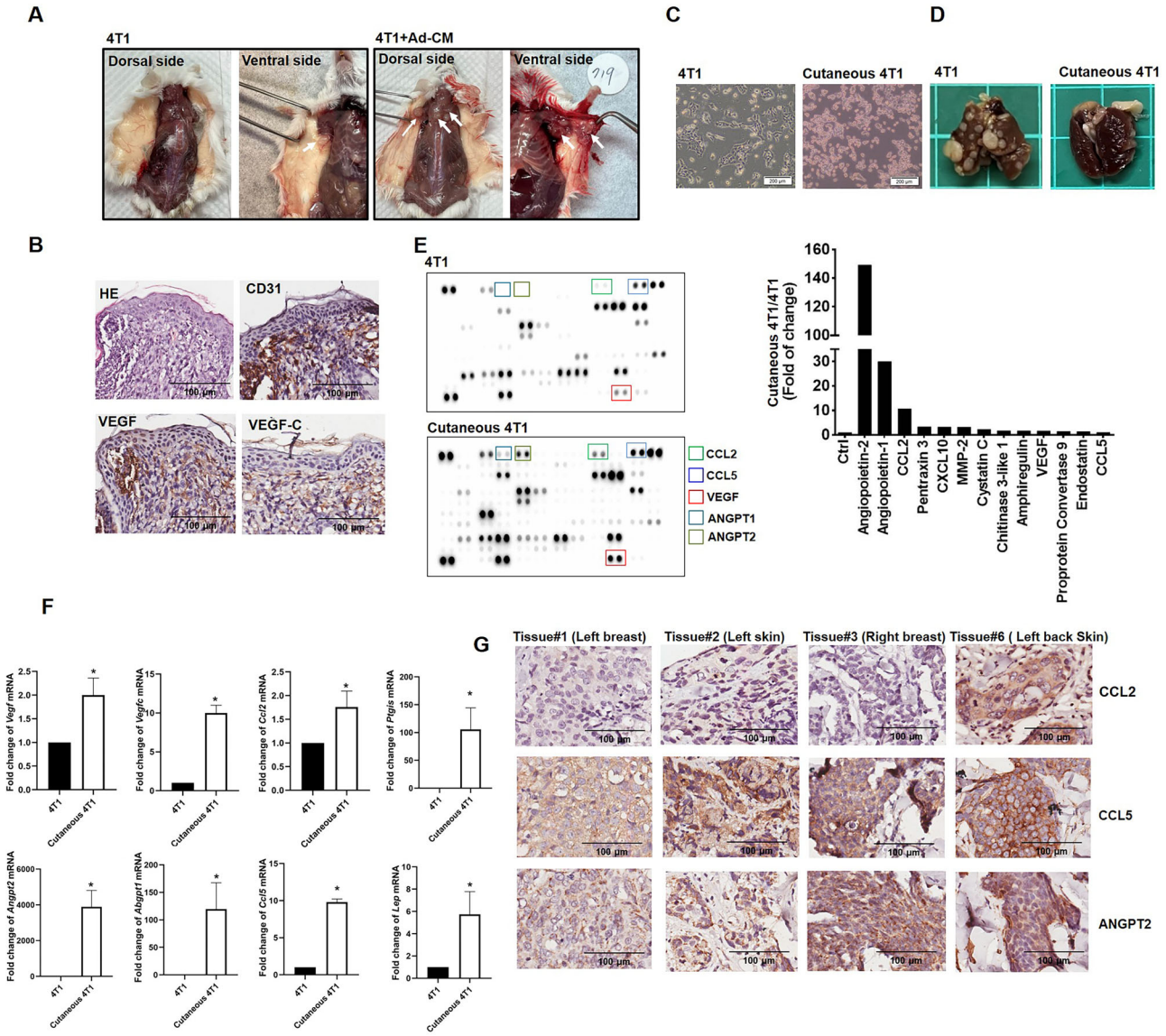

Fig. 4 | Cutaneous 4T1 cells exhibit the angiogenic and skin-metastatic properties characteristic of breast cancer cells. A Primary 4T1 cells were subcutaneously implanted into immunocompromised mice, allowed to form tumors, and surgically removed upon reaching 100-150 mm^3 tumor size. Post-surgery mice were monitored for two weeks while daily intraperitoneal injections of adipocyte-conditioned medium were administered. After two weeks, mice were dissected to examine tumor recurrence on the dorsal and ventral sides. **B** Hematoxylin and eosin (H&E) staining and IHC staining of VEGF, CD31, and VEGFC in cutaneous tumor tissues of mice. **C** Microscopic cell morphology of 4T1 and cutaneous 4T1 cells. **D** Comparison of Lung Metastasis Induced by Parental and Cutaneous 4T1 Cells in Mice. **E** Mouse Cytokine Antibody Array Kits (R&D) were applied to measure the content of 111 cytokines in the 4T1 and cutaneous 4T1 cells. Cytokines upregulated in cutaneous 4T1 and indicated by colored boxes are VEGF (red), CCL2 (green), CCL5 (blue), ANGPT 1 (light blue), and ANGPT2 2 (dark green). Highlighted rectangles indicate the cytokines elevated. **F** An RT-qPCR analysis of *Vegf*, *Vegfc*, *Ccl2*, *Ccl5*, *Angpt1*, *Angpt2*, *Lep*, and *Ptgis* mRNA expression in 4T1 and cutaneous 4T1 cells. Columns represent the mean results from PCR assays performed in triplicate and normalized to GAPDH (*$P < 0.05$). **G** IHC staining of CCL-2, CCL5, and ANGPT2 in tumor and cutaneous tumor tissues of the patient.

invasive tumors, with cancer cells exhibiting characteristic invasive morphology and elevated expression of angiogenic markers, including VEGF, VEGFC, and CD31 (Fig. 4B). These findings suggest that interactions between metastatic breast cancer cells and adipocytes may facilitate the aggressive behavior of CM, likely through the secretion of pro-angiogenic and tumor-promoting factors. This highlights the pivotal role of obesity-associated molecules in cancer progression.

We isolated and cultured cells from metastatic skin lesions to further characterize cutaneous metastatic cells. Compared with parental 4T1 cells, the cutaneous 4T1 cells exhibited a smaller, more rounded morphology (Fig. 4C). Next, we assessed cancer stem cell traits and anoikis resistance to determine the malignancy of cutaneous metastatic cells relative to their parental counterparts. As shown in Fig. S4A- S4C, cutaneous metastatic cells demonstrated enhanced sphere-forming capacity, increased $CD44^{high}/CD24^{low}$ subpopulations, and greater resistance to anoikis, indicating a more stem-like and resilient phenotype. Notably, when injected into mice, cutaneous 4T1 cells displayed a higher propensity for skin metastasis and a reduced tendency to colonize the lungs, in contrast to parental 4T1 cells, which predominantly metastasize to the lungs (Fig. 4D).

To explore the molecular basis for this phenotype, cytokine array analysis was performed on conditioned media from cutaneous versus parental 4T1 cells. Elevated levels of pro-tumorigenic factors, including Angiopoetin 1 (ANGPT1), Angiopoetin 2 (ANGPT2), CCL2, matrix metalloproteinases 2 (MMP2), and VEGF, were detected in cutaneous 4T1 cells (Fig. 4E). These results were validated by RT-qPCR (Fig. 4F), which confirmed upregulation of *Vegf, Vegfc*, *Ccl2*, *Ccl5*, *Angpt1/2*, *Lep*, and

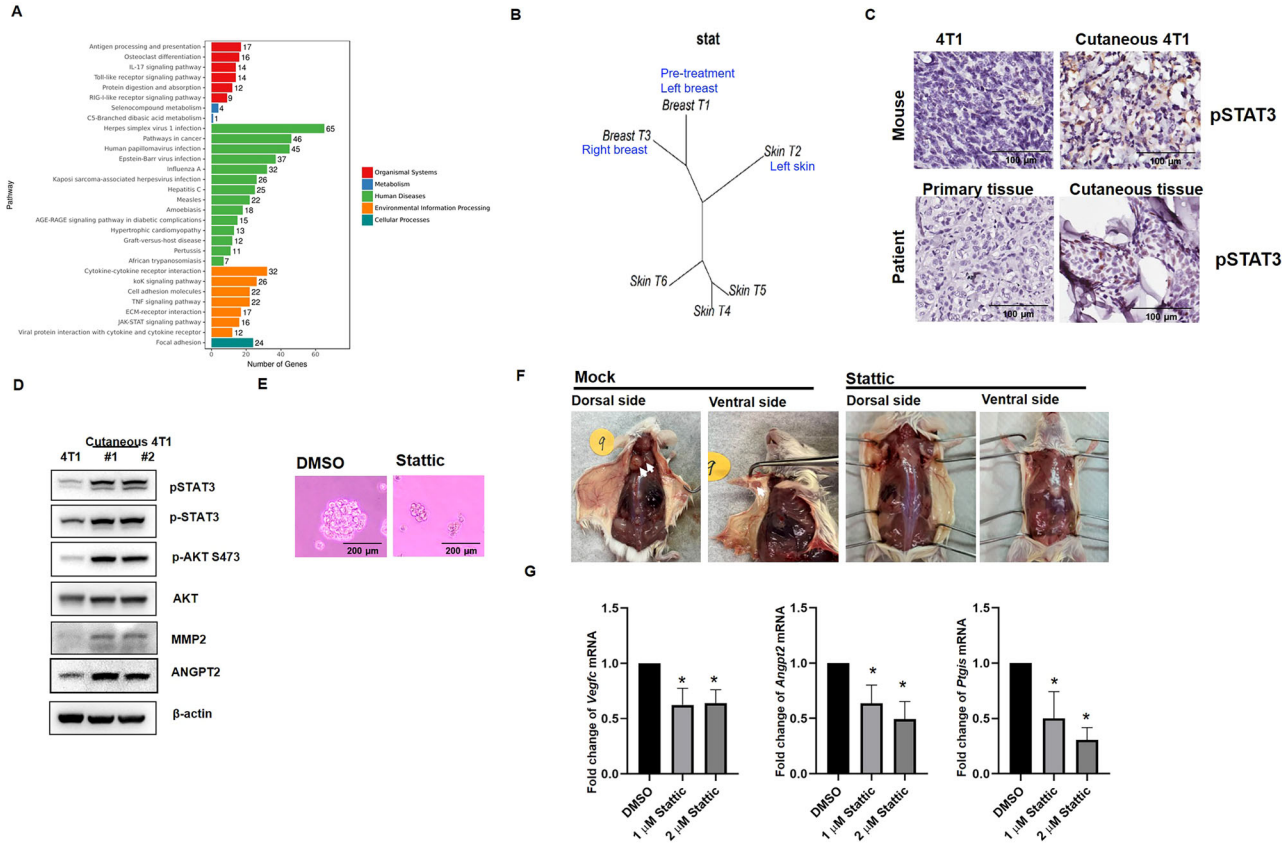

Fig. 5 | Inhibition of the JAK-STAT axis attenuates CMBC formation. A KEGG analysis of all differentially expressed genes in 4T1 and cutaneous 4T1. **B** A phylogenetic tree was constructed to compare stat-related pathway-associated genes (17 genes) across tumor tissues at different stages. **C, D** The levels of p-STAT3, STAT3, pAKT, AKT, MMP2, and ANGPT2 were determined by Western blot analysis, with β-actin serving as the loading control. **D** Comparison of p-STAT3 expression between 4T1 and cutaneous 4T1 cells, as well as between patient-derived primary tumor tissue and skin metastatic tissue, using immunohistochemistry. **E** Microscopic cell morphology of cutaneous 4T1 cells treated with Stattic after 5 days of culture in an ultra-low attachment dish. **F** Cutaneous 4T1 cells were subcutaneously implanted into immunocompromised mice and allowed to form tumors. Once tumors reached a volume of 100-150 mm^3, they were surgically excised. To evaluate tumor recurrence, mice were treated intraperitoneally with Stattic at a dosage of 10 mg/kg, administered three times per week for a duration of three weeks. After the treatment period, mice were sacrificed and examined for tumor recurrence on both the dorsal and ventral sides. **G** Quantitative RT-PCR analysis showing the expression levels of *Vegfc*, *Angpt2*, and *Ptgis* in cutaneous 4T1 cells after 3 days of Stattic treatment. Columns represent the mean results from PCR assays performed in triplicate and normalized to GAPDH ($^*p < 0.05$).

Ptgis. Notably, immunohistochemical staining of serial patient tissues demonstrated increased expression of CCL2, CCL5, and ANGPT2 in advanced lesions (Fig. 4G), linking experimental findings with clinical disease progression.

Inhibition of the JAK–STAT pathway attenuates the aggressiveness of CMBC cells

To further elucidate the mechanisms driving CM in breast cancer, we compared transcriptomic profiles between parental 4T1 cells and their skin-metastatic derivatives. As shown in Fig. 5A, pathway enrichment analysis identified significant upregulation of the JAK-STAT signaling cascade, cytokine-cytokine receptor interaction, and focal adhesion in cutaneous 4T1 cells, implicating the JAK-STAT axis in skin-tropic tumor progression. To validate these findings in a clinical context, we analyzed STAT gene expression across six patient-derived samples. As shown in Fig. 5B, primary tumors (Tissue #1 and #3) clustered distinctly from cutaneous metastatic lesions based on STAT-related gene expression, suggesting STAT pathway activation as a hallmark of CM. Further analysis of phosphorylated STAT3 (pSTAT3) expression revealed elevated levels in both cutaneous 4T1 cells and patient-derived cutaneous tissue samples, compared to parental 4T1 cells and the primary tumor (in situ) tissue (Fig. 5C).

Protein-level analysis further confirmed upregulated pSTAT3 and pAKT (S473) in cutaneous 4T1 cells, along with increased expression of the metastasis- and angiogenesis-related genes MMP2 and ANGPT2 (Fig. 5D). Functionally, treatment with the Stattic, a STAT3 inhibitor, significantly impaired spheroid formation, indicating that JAK-STAT signaling is essential for maintaining the stem-like phenotype of cutaneous metastatic cells (Fig. 5E). In vivo administration of Stattic markedly reduced subcutaneous tumor burden, especially in the dorsal neck region, compared to controls (Fig. 5F). Consistently, RT-qPCR demonstrated that Stattic treatment significantly downregulated *Vegfc*, *Angpt2*, and *Ptgis* expression (Fig. 5G).

Collectively, these data demonstrate that activation of the JAK-STAT pathway supports the aggressive and metastatic behavior of cutaneous breast cancer cells, and that STAT3 inhibition may represent a promising therapeutic strategy for managing skin-dominant metastatic breast cancer.

Validation of angiogenic and metabolic gene signatures associated with CMBC and clinical outcomes

To validate the role of angiogenic, cytokine, and fatty acid metabolism genes in CMBC, we conducted a small-scale validation study using tissue samples from 6 patients with no metastasis, 6 with non-cutaneous metastasis, and 15 with cutaneous metastases including 6 with cutaneous metastasis only and 9 with both skin and visceral metastases (multiple-organ metastasis) to assess the expression of *STAT3*, *ANGPT2*, *VEGFC*, *PTGIS*, and *LEP*. As illustrated in Fig. 6A, Gene expression profiling revealed significantly elevated levels of *STAT3* and *PTGIS* in the CM group compared to both non-cutaneous and

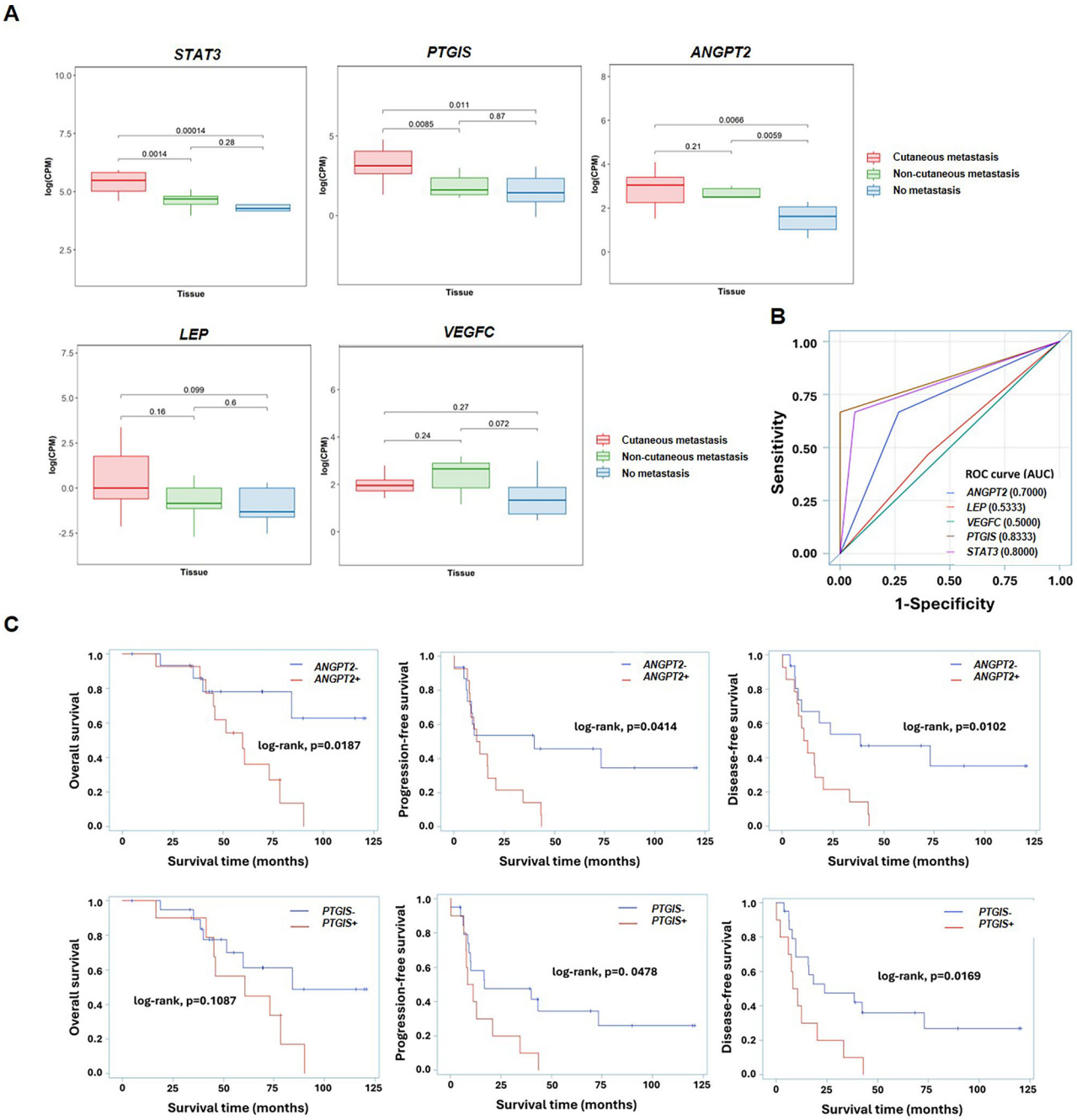

Fig. 6 | Correlation analysis of angiogenesis-, cytokine-, and fatty acid metabolism-related genes in CMBC. A Boxplot showing *STAT3*, *LEP*, *PTGIS*, *ANGPT2*, and *VEGFC* mRNA expression levels (logCPM) in tissues from three patient groups: cutaneous metastasis (red), non-cutaneous metastasis (green), and no metastasis (blue). **B** The ROC curve shows the diagnostic ability of biomarkers *STAT3*, *LEP*, *PTGIS*, *ANGPT2*, and *VEGFC* to distinguish between CM and non-CM states. **C** Kaplan-Meier survival analysis comparing OS between *STAT3*, *PTGIS*, and *ANGPT2*-positive and *STAT3*, *PTGIS*, and *ANGPT2*-negative patient groups.

no metastasis cohorts ($P < 0.001$), indicating a strong association with skin-specific metastasis (Fig. 6A). While *ANGPT2* and *LEP* showed increased expression trends in cutaneous samples, statistical significance was not achieved. Similarly, *VEGFC* was mildly elevated in metastatic groups but failed to reach statistical thresholds. To assess the predictive potential of these biomarkers, ROC curve analysis was conducted (Fig. 6B). *PTGIS* and *STAT3* demonstrated the highest discriminatory power for predicting CM, with AUC values of 0.8333 and 0.8000, respectively. *ANGPT2* yielded moderate performance (AUC = 0.7000), whereas *LEP* and *VEGFC* exhibited AUC values close to random chance (0.5333 and 0.5000), suggesting limited utility as classifiers. *PTGIS* and *STAT3* demonstrated superior classification performance compared to the other biomarkers.

Next, we further assessed the association between the expression levels of five genes (*STAT3*, *ANGPT2, PTGIS, VEGFC*, and *LEP*) and patient survival using Kaplan-Meier plots. As shown in Fig. 6C, *STAT3*, *ANGPT2*, and *PTGIS* expression levels demonstrated statistically significant differences in survival outcomes. Patients with high *STAT3*, *ANGPT2*, or *PTGIS* expression (*STAT3*+, *ANGPT2*+, or *PTGIS*+) exhibited significantly worse PFS and DFS compared to those with lower expression, suggesting that these genes may serve as negative prognostic markers and potential biomarkers for poor clinical outcomes (Fig. 6C). In contrast, while high *VEGFC* expression was associated with a trend toward poorer OS, PFS, and DFS, these differences did not reach statistical significance. Similarly, *LEP* expression did not significantly impact survival outcomes, although a subtle trend toward worse

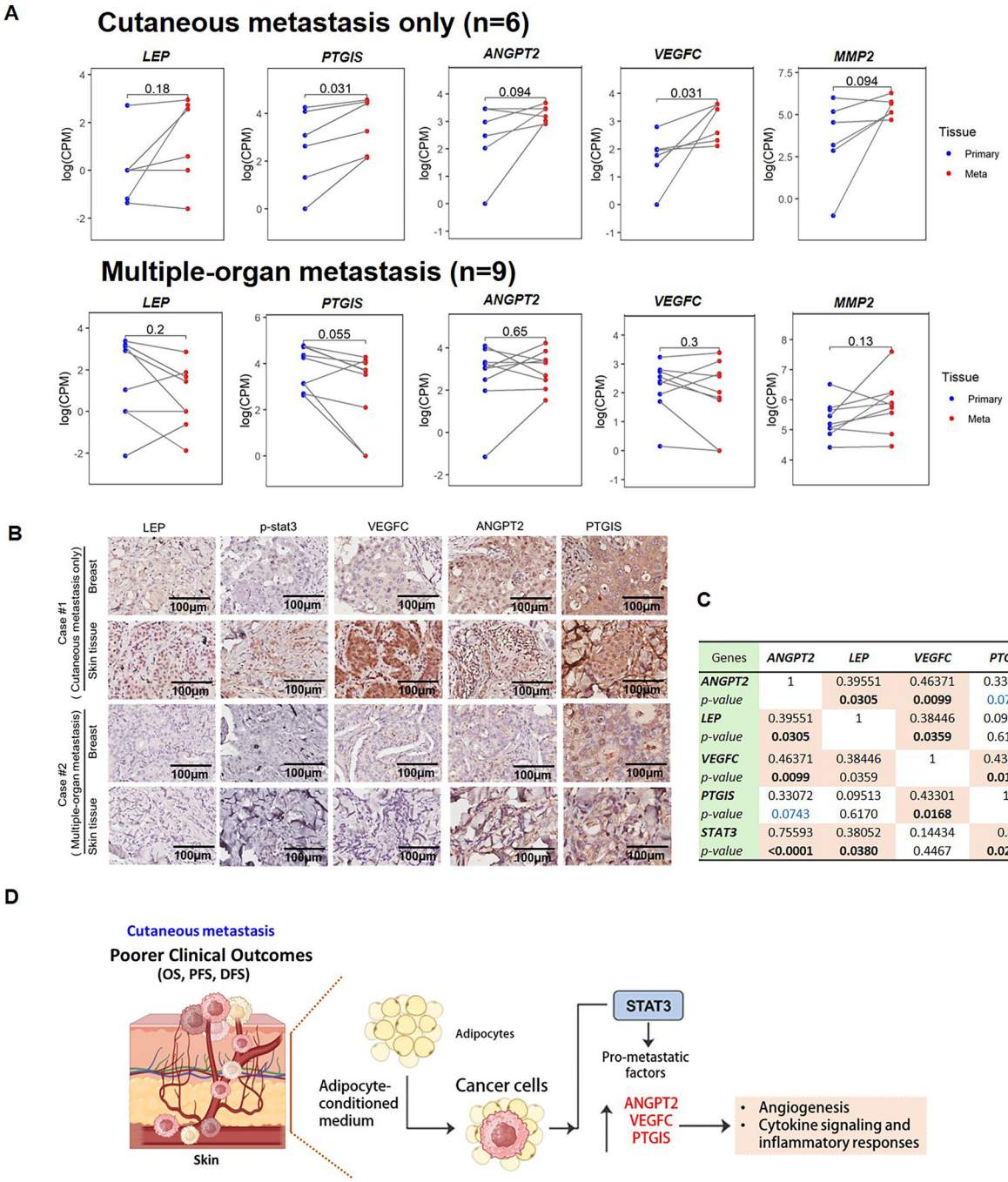

Genes	*ANGPT2*	*LEP*	*VEGFC*	*PTGIS*	*STAT3*
ANGPT2	1	0.39551	0.46371	0.33072	0.75593
p-value		**0.0305**	**0.0099**	0.0743	**<0.0001**
LEP	0.39551	1	0.38446	0.09513	0.38052
p-value	**0.0305**		**0.0359**	0.6170	**0.0380**
VEGFC	0.46371	0.38446	1	0.43301	0.14434
p-value	**0.0099**	0.0359		**0.0168**	0.4467
PTGIS	0.33072	0.09513	0.43301	1	0.40000
p-value	0.0743	0.6170	**0.0168**		**0.0285**
STAT3	0.75593	0.38052	0.14434	0.4	1
p-value	**<0.0001**	**0.0380**	0.4467	**0.0285**	

Fig. 7 | Elevated expression of pro-metastatic genes in cutaneous metastases compared to primary breast tumors. A Paired dot plot comparing *LEP, PTGIS, ANGPT2, VEGFC*, and *MMP2* mRNA expression levels (logCPM) between primary tumor tissues (blue) and corresponding metastatic tissues (red) from the same patients with cutaneous metastasis only ($n = 6$) and multiple-organ metastasis ($n = 9$). **B** Immunohistochemical staining of LEP, p-STAT3, VEGFC, PTGIS, and ANGPT2 in patient-derived tumor and metastatic skin tissues. **C** Pearson analysis of the relation among *STAT3*, *LEP*, *VEGFC*, *PTGIS*, and *ANGPT2*. **D** STAT3-PTGIS-ANGPT2 signaling axis as a key promoter of skin-homing behavior in breast cancer cells.

prognosis in *LEP*+ patients was observed (Fig. S5). Further studies with larger cohorts are warranted to validate these findings.

Distinct upregulation of angiogenic and metabolic genes in skin-only metastatic lesions

To further elucidate the molecular landscape of cutaneous metastases, we analyzed paired primary and skin metastatic tumor samples from breast cancer patients. As shown in Fig. 7A, patients with cutaneous metastasis only ($n = 6$) exhibited significantly elevated expression of *PTGIS* ($P = 0.031$) and *VEGFC* ($P = 0.031$) in metastatic tissues compared to their matched primary tumors. Expression levels of *ANGPT2* and *MMP2* also showed upward trends ($P < 0.1$), while *LEP* exhibited a moderate, though non-significant, increase. In contrast, patients with multiple-organ metastasis ($n = 9$) with both cutaneous and visceral spread displayed minimal differences in gene expression between primary and metastatic sites. Protein-level validation using IHC staining of tissue samples further supported the transcriptomic findings (Fig. 7B). Notably, a patient with cutaneous metastasis only (Case #1) exhibited enhanced staining for p-STAT3, VEGFC, ANGPT2, and PTGIS in metastatic tissue, whereas these markers were less prominent in the skin lesions of a patient with multi-organ

involvement (Case #2). Finally, Pearson correlation analysis revealed strong positive associations among *ANGPT2*, *PTGIS*, *STAT3*, *VEGFC*, and *LEP* expression (Fig. 7C), suggesting potential co-regulation among these angiogenesis- and metabolism-related genes. These results indicate that during CM in breast cancer, these genes/proteins may play interrelated and potentially co-regulatory roles (Fig. 7D). Collectively, these results support the hypothesis that cutaneous metastasis only breast cancer represents a distinct molecular subtype characterized by coordinated upregulation of pro-angiogenic and inflammatory pathways.

Discussion

This study highlights novel pathways associated with the cutaneous metastatic phenotype in breast cancer. Through RNA-seq analysis of patient-derived skin tissues and in vivo models, we identified marked upregulation of genes linked to fatty acid metabolism and angiogenesis in CMBC. Several growth factors and cytokines implicated in these pathways may contribute to tumor progression and metastasis within the skin microenvironment. Our findings suggest that hypercytokinemia, characterized by excessive cytokine production, is a hallmark of CMBC. Targeting this dysregulated cytokine activity may offer new opportunities for personalized therapies, particularly for skin metastases. Although validation was performed using 4T1-derived cutaneous cell lines, our clinical tissue cohort included specimens from HER2+, luminal, and TNBC metastatic breast cancer patients. Thus, our findings broadly support the relevance of these mechanisms in both non-TNBC and TNBC cutaneous metastases.

Lymphangiogenesis plays a central role in CM development. Elevated lymphatic vessel density around primary tumors and within metastatic sites, including the skin, correlates with enhanced cancer dissemination. VEGFC and VEGFD, two key pro-lymphangiogenic factors, promote lymphatic growth and facilitate metastatic spread via the lymphatic system. Their increased expression is consistently observed in both primary and metastatic cutaneous lesions[22]. Additionally, pro-inflammatory cytokines such as IL-6, IL-8, and TGF-β contribute to tumor growth, immune evasion, and angiogenesis [23]. Overexpression of cytokine receptors, including IL-6R, CXCR4, CCR7, and CCR10, is also common in metastatic breast cancer, particularly at cutaneous sites. Their ligands (CXCL12, CCL19, CCL21, and CCL27) further promote cancer cell adhesion, migration, and survival[10–12]. We also observed elevated expression of the angiopoietin-Tie signaling axis in CM skin tissues, reinforcing the importance of targeting VEGFC, VEGFD, angiopoietin, and their receptors as a therapeutic strategy under investigation in preclinical models.

Breast tissue's high adipose content plays a significant role in tumor biology. In our murine CM model, breast cancer cells preferentially metastasized to BAT-rich areas, including the neck, interscapular, and paraspinal regions. BAT, known for non-shivering thermogenesis, also functions as an endocrine organ, secreting batokines such as FGF21 and IL-6 that influence angiogenesis, metabolism, and inflammation[24]. These factors may create a favorable microenvironment for cancer cell colonization and survival[25,26]. In pathological states like obesity, BAT secretory dysfunction may exacerbate tumor progression. Co-culture of breast cancer cells with autologous adipocytes led to increased expression of *LEP* and *S1PR1*, highlighting tumor-adipocyte interactions that promote angiogenesis. LEP, commonly elevated in obesity, contributes to tumor growth and metastasis[27–29]. S1PR1, activated by elevated sphingosine-1-phosphate in obesity, drives metastatic behavior in breast cancer[30–32]. Adipokine imbalance, including altered LEP and adiponectin, may further enhance S1P/S1PR1 signaling and promote aggressiveness in obese individuals.

Transcriptomic data revealed dysregulation of fatty acid metabolism, particularly AA and LA pathways, in CM skin tissues. Linoleic acid, an omega-6 PUFA, is metabolized into pro-inflammatory lipids that promote inflammation, angiogenesis, and invasion[33,34]. These effects are mediated through ECM remodeling via MMPs, which degrade structural barriers and facilitate invasion[35,36]. LA-derived metabolites also enhance neovascularization[37]. Genes such as *ACSBG1*, *ACADL*, *ACADSB*, and *SCD5*, alongside *PTGS2*, *LTC4S*, and *PTGIS*, were significantly upregulated. Elevated expression of PLA2G family members (e.g., *PLA2G2A*, *PLA2G2C*, *PLA2G4A*) indicates heightened phospholipid metabolism and signaling activity. Concurrently, decreased GPX1 expression may elevate ROS, promoting inflammation and DNA damage[38]. Similarly, loss of CBR3 may lead to accumulation of toxic aldehydes like 4-HNE, contributing to genomic instability[39] and adaptation of metastatic cells to the cutaneous niche[40]. Recent studies suggest that ω-6 LA may activate mTORC1 in a FABP5-dependent manner, particularly in TNBC. Elevated FABP5 and ω-6 PUFA levels in TNBC patients further highlight dietary lipid involvement and therapeutic implications[41]. Targeting key enzymes in LA metabolism or their downstream pathways may hold promise for suppressing metastasis in CMBC.

JAK2 and STAT3 are among the genes that are preferentially mutated in metastatic breast cancer, suggesting that targeting the JAK/STAT pathway could be a promising strategy for future therapies[19]. Activation of STAT3 is known to promote adipocyte differentiation and regulate the secretion of adipokines, which in turn can influence the tumor microenvironment[42]. JAK2/STAT3 is activated by pro-inflammatory cytokines (such as IL-6), mediating innate and adaptive immune responses that often create a supportive niche for tumor growth. Furthermore, STAT3 activation is closely linked to angiogenesis through the upregulation of pro-angiogenic factors such as VEGF, thereby facilitating the formation of new blood vessels that supply the tumor with oxygen and nutrients[43]. Notably, previous studies have identified the leptin-STAT3-G9a axis as a driver of cancer stem-like cell formation in breast cancer, particularly under conditions of obesity[44]. Our data further suggests that PTGIS is central to this regulatory network. Supporting this, prior studies have demonstrated that pharmacologic inhibition of PTGIS not only reduces phosphorylated STAT3 (p-STAT3) relative to total STAT3 levels across multiple basal-like breast cancer cell lines, but also impairs the growth of $CD44^{+}CD24^{-}$ breast cancer stem-like cells[23,45]. These findings collectively highlight the STAT3-PTGIS signaling axis as a critical mediator of tumor progression and a potential target for anticancer therapy. Consistent with these observations, we found that breast cancer cells exhibiting a cutaneous metastatic phenotype displayed markedly elevated p-STAT3 levels. Inhibition of STAT3 activation significantly suppressed both tumor growth and the formation of CMs. Therefore, targeting the JAK2/STAT3 pathway may represent an effective and personalized therapeutic strategy in CMBC, potentially attenuating adipocyte-derived pro-tumorigenic signaling, reducing chronic inflammation, and inhibiting angiogenesis.

Methods

RNA-Seq data analysis

One microgram of total RNA was used to prepare the mRNA libraries. Poly(A)-mRNA was isolated using oligo (dT) beads and fragmented using divalent cations at high temperatures. Random Primers were used, followed by first- and second-strand cDNA syntheses. Double-stranded cDNA was purified, and end repair and dA-tailing were performed in a single reaction. Adaptors were ligated to both ends using T-A ligation. The adaptor-ligated DNA was size-selected using clean DNA beads. The samples were then amplified by PCR using primers P5 and P7, and the PCR products were validated for quality. Indexed libraries were multiplexed and sequenced on an Illumina HiSeq, Novaseq, or MGI2000 system using a 2 × 150 paired-end (PE) configuration according to the manufacturer's instructions. Fastq data were processed using Cutadapt (v1.9.1) to remove technical sequences, such as adapters, PCR primers, and low-quality bases (Phred score < 20). Only the high-quality reads (75 bp) were retained for further analysis. Reference genomes and gene annotations were downloaded from the UCSC, NCBI, or ENSEMBL databases. Hisat2 (v2.2.1) was used to index the reference genome and align the high-quality reads to the reference genome. Transcripts were generated from off-annotation files. HTSeq (v0.6.1) was used to estimate gene and isoform expression levels from clean PE reads using the converted transcripts as reference files. Differential gene expression analysis was performed using the DESeq2 Bioconductor package based on a negative binomial distribution. Logarithmic fold-

changes and dispersion estimates were adjusted using data-driven priors. Genes with an adjusted *p*-value (Padj) ≤ 0.05 were considered differentially expressed.

KEGG enrichment analysis

We used the Kyoto Encyclopedia of Genes and Genomes (KEGG) database, Reactome (37941124), and SRplot (37943830), which compiles information on genomes, biological pathways, diseases, drugs, and chemical substances, for pathway analysis. In-house scripts were developed to identify and enrich DEGs within the KEGG pathways, enabling a deeper understanding of the underlying molecular mechanisms and potential interactions.

Gene set enrichment and modeling of gene interaction networks

Upregulated genes were analyzed using Ingenuity Pathways Analysis (IPA) software (Ingenuity Systems, www.ingenuity.com) and subjected to functional annotation and regulatory network analysis. The analysis included several prediction algorithms, including Upstream Regulator Analysis (URA), Downstream Effects Analysis (DEA), mechanistic network (MN), and Causal Network Analysis (CNA). IPA employs these algorithms to predict functional regulatory networks from gene expression data. It assigns a significance score to each network based on its relevance to the input set of focus genes. Significance was calculated as the negative logarithm of the *p*-value, representing the likelihood that the observed grouping of focus genes in the network occurred by chance. This method facilitates the identification of critical regulators and pathways involved in the biological processes under investigation.

Immunohistochemistry

Immunohistochemistry staining was performed to detect target proteins in patient tissue samples. Tissue sections (4-5 μm thick) were obtained from paraffin-embedded blocks and mounted on slides. After deparaffinization in xylene and rehydration with ethanol, antigen retrieval was performed using sodium citrate buffer (pH 6.0) with heat for 10-20 min. Endogenous peroxidases were blocked with 3% hydrogen peroxide, followed by blocking with serum to reduce nonspecific binding. Sections were incubated with the primary antibody overnight at 4 °C. After rinsing, a biotinylated secondary antibody was applied at room temperature for 30-60 min. Detection was performed using an enzyme-labeled complex (ABC), followed by DAB staining. Finally, the sections were counterstained with hematoxylin, dehydrated, cleared, and mounted for analysis.

Flow cytometry for apoptosis

Briefly, cells were prepared by either trypsinizing the adherent cells or collecting the suspended cells directly. The cell suspension was centrifuged at 300 *g* for 5 min to pellet the cells, and the pellet was washed once with PBS. The cells were resuspended in Annexin V-binding buffer at a concentration of 1×10^6 cells/mL. Subsequently, 100 μL of the cell suspension (about 1×10^5 cells) was aliquoted into a new tube, and five μL of Annexin V-FITC was added. The mixture was incubated in the dark for 15 min at room temperature. After that, five μL of propidium iodide was added, typically at a concentration of 50 μg/mL, and incubated for another 5 min at room temperature in the dark. Finally, 400 μL Annexin V binding buffer was added to each tube and mixed gently. The stained cells were immediately analyzed using a flow cytometer.

Endothelial cell tube formation

First, cancer cells were seeded in a culture dish at 60-70% confluency. At 70-80% confluency, they were washed twice with PBS to remove serum, and serum-free medium was added, followed by incubation for 24-48 h. The conditioned medium was then collected. Matrigel was prepared by thawing on ice overnight and keeping the tools cold to prevent premature solidification. Matrigel was added to a 24-well plate and incubated at 37 °C for 30-60 min for solidification. Endothelial cells were harvested, resuspended in a 1:1 mixture of endothelial cell culture medium and cancer cell-conditioned medium, and seeded on top of the solidified Matrigel at a density of 3×10^4-5×10^4 cells/well. The plate was incubated at 37 °C for 4-8 h, during which tube-like structures formed.

In vivo orthotopic mouse model

Primary 4T1 cells (1×10^6) were implanted into the fourth mammary fat pad of female BALB/c mice. Tumors were allowed to develop until they reached a volume of 100-150 mm^3, after which surgical resection was performed under sterile conditions to ensure complete removal of the primary tumor. Following surgery, the mice were monitored for four weeks to evaluate local tumor recurrence. During this observation period, the animals received daily intraperitoneal injections of 100 μL adipocyte-conditioned medium (Ad-CM). Ad-CM was prepared from cultured adipocytes, centrifuged at 300 *g* for 10 min to remove cells, followed by 2000 *g* for 10 min to remove debris, and then either used immediately or stored at −80 °C until use. To specifically assess the role of JAK-STAT signaling in tumor recurrence, mice were additionally implanted with cutaneous 4T1 cells and treated intraperitoneally with Stattic (10 mg/kg), administered three times per week for three weeks. Drug injections were performed under inhalational anesthesia with 2% isoflurane to minimize animal discomfort. At the end of the four-week postoperative period, mice entered the skin metastasis evaluation stage. Animals were euthanized by CO_2 inhalation, and tissues were harvested for histological and molecular analyses.

Statistical analysis

Statistical analyses and graphing were performed using the GraphPad Prism 8.0 software (GraphPad, San Diego, CA, USA). A Z score ($2.0 \leq Z \geq 2.0$) was considered significant for IPA analyses.

Ethics statement

Informed consent was obtained from all participants in this study. The consent process followed the ethical guidelines outlined in the Declaration of Helsinki, and the study was approved by the Research Ethics Committee of Kaohsiung Medical University Hospital KMUHIRB-G(I)-20200039, KMUHIRB-G(II)-20190005, and KMUHIRB-G(II)-20170030. All experimental methods were performed following the guidelines of Kaohsiung Medical University Hospital. Animal experimental procedures were reviewed and approved by the Institute of Animal Care and Use Committee at Kaohsiung Medical University (IACUC no. 109114 and no. 112102). They were performed under the Guide for the Care and Use of Laboratory Animals. Animals were housed in an Association for Assessment and Accreditation of Laboratory Animal Care International (Frederick, MD, USA) approved animal facility at Kaohsiung Medical University.

Data availability

The data supporting this study's findings are available from the corresponding author upon reasonable request.

Received: 29 July 2025; Accepted: 6 November 2025;
Published online: 06 February 2026

References

1. Nava, G., Greer, K., Patterson, J. & Lin, K. Y. Metastatic cutaneous breast carcinoma: A case report and review of the literature. *Cancer J. Plast. Surg.* **17**, 25–27 (2009).
2. Spencer, P. S. & Helm, T. N. Skin metastases in cancer patients. *Cutis* **39**, 119–121 (1987).
3. Alcaraz, I., Cerroni, L., Rütten, A., Kutzner, H. & Requena, L. Cutaneous metastases from internal malignancies: a clinicopathologic and immunohistochemical review. *Am. J. Dermatopathol.* **34**, 347–393 (2012).
4. Guanziroli, E. et al. Cutaneous metastases of internal malignancies: an experience from a single institution. *Eur. J. Dermatol* **27**, 609–614 (2017).

5. Tan, A. R. Cutaneous manifestations of breast cancer. *Semin Oncol.* **43**, 331–334 (2016).
6. Dadras, S. S. & Detmar, M. Angiogenesis and lymphangiogenesis of skin cancers. *Hematol. Oncol. Clin. North Am.* **18**, 1059–1070 (2004).
7. Otsuka, I. Cutaneous metastasis after surgery, injury, lymphadenopathy, and peritonitis: possible mechanisms. *Int. J. Mol. Sci*. **20**, https://doi.org/10.3390/ijms20133286 (2019).
8. Varricchi, G., Granata, F., Loffredo, S., Genovese, A. & Marone, G. Angiogenesis and lymphangiogenesis in inflammatory skin disorders. *J. Am. Acad. Dermatol* **73**, 144–153 (2015).
9. Kunstfeld, R. et al. Induction of cutaneous delayed-type hypersensitivity reactions in VEGF-A transgenic mice results in chronic skin inflammation associated with persistent lymphatic hyperplasia. *Blood* **104**, 1048–1057 (2004).
10. Müller, A. et al. Involvement of chemokine receptors in breast cancer metastasis. *Nature* **410**, 50–56 (2001).
11. Tiberio, L. et al. Chemokine and chemotactic signals in dendritic cell migration. *Cell Mol. Immunol.* **15**, 346–352 (2018).
12. Zlotnik, A. & Yoshie, O. The chemokine superfamily revisited. *Immunity* **36**, 705–716 (2012).
13. Wang, Q. et al. Role of tumor microenvironment in cancer progression and therapeutic strategy. *Cancer Med* **12**, 11149–11165 (2023).
14. Cirillo, D., Rachiglio, A. M., la Montagna, R., Giordano, A. & Normanno, N. Leptin signaling in breast cancer: an overview. *J. Cell Biochem* **105**, 956–964 (2008).
15. Hillers-Ziemer, L. E. et al. Obesity Promotes Cooperation of Cancer Stem-Like Cells and Macrophages to Enhance Mammary Tumor Angiogenesis. *Cancers* **12**, https://doi.org/10.3390/cancers12020502 (2020).
16. Xu, Y. et al. Molecular alterations and prognosis of breast cancer with cutaneous metastasis. *Diagn. Pathol.* **19**, 93 (2024).
17. Schrijver, W. et al. Mutation profiling of key cancer genes in primary breast cancers and their distant metastases. *Cancer Res* **78**, 3112–3121 (2018).
18. González-Martínez, S. et al. Clinical, pathological, and molecular features of breast carcinoma cutaneous metastasis. *Cancers* **13**, https://doi.org/10.3390/cancers13215416 (2021).
19. Paul, M. R. et al. Genomic landscape of metastatic breast cancer identifies preferentially dysregulated pathways and targets. *J. Clin. Invest* **130**, 4252–4265 (2020).
20. Dirat, B. et al. Cancer-associated adipocytes exhibit an activated phenotype and contribute to breast cancer invasion. *Cancer Res* **71**, 2455–2465 (2011).
21. Hsieh, C. C., Wang, C. H. & Huang, Y. S. Lunasin attenuates obesity-associated metastasis of 4T1 breast cancer cell through anti-inflammatory property. *Int. J. Mol. Sci.* **17**, https://doi.org/10.3390/ijms17122109 (2016).
22. Cunnick, G. H. et al. Lymphangiogenesis and lymph node metastasis in breast cancer. *Mol. Cancer* **7**, 23 (2008).
23. Manore, S. G., Doheny, D. L., Wong, G. L. & Lo, H. W. IL-6/JAK/STAT3 signaling in breast cancer metastasis: biology and treatment. *Front Oncol.* **12**, 866014 (2022).
24. Cannon, B. & Nedergaard, J. Brown adipose tissue: function and physiological significance. *Physiol. Rev.* **84**, 277–359 (2004).
25. Villarroya, F., Cereijo, R., Villarroya, J. & Giralt, M. Brown adipose tissue as a secretory organ. *Nat. Rev. Endocrinol.* **13**, 26–35 (2017).
26. Hondares, E. et al. Thermogenic activation induces FGF21 expression and release in brown adipose tissue. *J. Biol. Chem.* **286**, 12983–12990 (2011).
27. Saxena, N. K. & Sharma, D. Multifaceted leptin network: the molecular connection between obesity and breast cancer. *J. Mammary Gland Biol. Neoplasia* **18**, 309–320 (2013).
28. Andò, S. et al. Obesity, leptin and breast cancer: epidemiological evidence and proposed mechanisms. *Cancers* **11**, https://doi.org/10.3390/cancers11010062 (2019).
29. Park, J., Euhus, D. M. & Scherer, P. E. Paracrine and endocrine effects of adipose tissue on cancer development and progression. *Endocr. Rev.* **32**, 550–570 (2011).
30. Pyne, N. J. & Pyne, S. Sphingosine 1-phosphate and cancer. *Nat. Rev. Cancer* **10**, 489–503 (2010).
31. Nagahashi, M. et al. Targeting the SphK1/S1P/S1PR1 axis that links obesity, chronic inflammation, and breast cancer metastasis. *Cancer Res.* **78**, 1713–1725 (2018).
32. Vona-Davis, L. & Rose, D. P. Angiogenesis, adipokines and breast cancer. *Cytokine Growth Factor Rev.* **20**, 193–201 (2009).
33. Nindrea, R. D., Aryandono, T. & Lazuardi, L. Breast cancer risk from modifiable and non-modifiable risk factors among women in Southeast Asia: A meta-analysis. *Asian Pac. J. Cancer Prev.* **18**, 3201–3206 (2017).
34. Lands, W. E. Dietary fat and health: the evidence and the politics of prevention: careful use of dietary fats can improve life and prevent disease. *Ann. N. Y Acad. Sci.* **1055**, 179–192 (2005).
35. Manosalva, C. et al. Free fatty acid Receptor 1 signaling contributes to migration, MMP-9 activity, and Expression of IL-8 induced by linoleic acid in HaCaT Cells. *Front Pharm.* **11**, 595 (2020).
36. Hubbard, N. E., Lim, D. & Erickson, K. L. Conjugated linoleic acid alters matrix metalloproteinases of metastatic mouse mammary tumor cells. *J. Nutr.* **137**, 1423–1429 (2007).
37. Nishioka, N. et al. Linoleic acid enhances angiogenesis through suppression of angiostatin induced by plasminogen activator inhibitor 1. *Br. J. Cancer* **105**, 1750–1758 (2011).
38. Brigelius-Flohé, R. & Maiorino, M. Glutathione peroxidases. *Biochim Biophys. Acta* **1830**, 3289–3303 (2013).
39. Nakamura, H. & Takada, K. Reactive oxygen species in cancer: Current findings and future directions. *Cancer Sci.* **112**, 3945–3952 (2021).
40. Zhang, M. et al. LncRNA CBR3-AS1 regulates of breast cancer drug sensitivity as a competing endogenous RNA through the JNK1/MEK4-mediated MAPK signal pathway. *J. Exp. Clin. Cancer Res.* **40**, 41 (2021).
41. Koundouros, N. et al. Direct sensing of dietary omega-6 linoleic acid through FABP5-mTORC1 signaling. *Science* **387**, eadm9805 (2025).
42. Yu, H., Pardoll, D. & Jove, R. STATs in cancer inflammation and immunity: a leading role for STAT3. *Nat. Rev. Cancer* **9**, 798–809 (2009).
43. Wei, D. et al. Stat3 activation regulates the expression of vascular endothelial growth factor and human pancreatic cancer angiogenesis and metastasis. *Oncogene* **22**, 319–329 (2003).
44. Chang, C. C., Wu, M. J., Yang, J. Y., Camarillo, I. G. & Chang, C. J. Leptin-STAT3-G9a signaling promotes obesity-mediated breast cancer progression. *Cancer Res.* **75**, 2375–2386 (2015).
45. Marotta, L. L. et al. The JAK2/STAT3 signaling pathway is required for growth of $CD44^{+}CD24^{-}$ stem cell-like breast cancer cells in human tumors. *J. Clin. Invest.* **121**, 2723–2735 (2011).

Acknowledgements

The following grants supported this work: 1) 114-2320-B-037 -002 -, 114-2314-B-037 -094 -, 114-2320-B-037 -001 -, 113-2320-B-037 005 -, 113-2320-B-037-006 -, 112-2314-B037-045-, 111-2314-B-650-006-MY3, 113-2811-B-037-001 -, 112-2320-B-037-002-, 112-2628-B-037-002-, and 112-2314-B-037-044 from the Ministry of Science and Technology, Taiwan. 2) KMUH-DK(C)111003 from the Kaohsiung Medical University, Kaohsiung, Taiwan. 3) KMUH113-3R34 from Kaohsiung Medical University Hospital, Kaohsiung, Taiwan. 4) The authors thank the Center for Laboratory Animals in Kaohsiung Medical University for the animal care.

Author contributions

Luo CW and Pan MR collected and designed the research and wrote and edited the manuscript; OY Fu, Wu CC and Chu WL collected patient information. Moi SH, Chang SJ, and Hung YH Performed statistical analyses. Hsu MH, Yang YT, Chen YZ, and Wu CC did the formal analysis, data curation, and conceptualization. Li YL, Hung WC, Lin SY, Li WP, and Hou MF were involved in the investigation. All authors reviewed the manuscript.

Competing interests
The authors declare no competing interests.

Additional information
Supplementary information The online version contains supplementary material available at https://doi.org/10.1038/s41698-025-01184-1.

Correspondence and requests for materials should be addressed to Mei-Ren Pan.